Smart Mater. Struct. **7** (1998) 305–311. Printed in the UK PII: S0964-1726(98)91230-7

Evaluation of a surface acoustic wave motor with a multi-contact-point slider

Minoru Kuribayashi Kurosawa†, Makoto Chiba and Toshiro Higuchi

Department of Precision Machinery Engineering, Graduate School of Engineering, The University of Tokyo, Japan

Received 27 July 1997, accepted for publication 17 October 1997

Abstract. Previously, the surface acoustic wave linear motor has been demonstrated and its exact pre-load conditions investigated. Based on this previous research, multi-contact-point sliders were designed and tested. A maximum output force of 0.45 N, 450 times that obtained in preliminary experiments, was successfully obtained. Simple simulation results predicted that much larger thrust would be available by increasing the actual contact point area without changing the slider and the stator dimensions. The calculated output force was 10 N, roughly twenty times that observed experimentally. To realize the required stator texture of the contact surface, a silicon micro-machining technique or other conventional methods would be applicable.

1. Introduction

Surface acoustic wave devices are widely used in communication instruments. These devices are operated at high-energy-density conditions in order to save materials and space. As is well known, the energy density of piezoelectric devices is roughly in proportion to the operating frequency. Thus the use of surface acoustic wave devices as actuators at high-frequency operation conditions can be expected to produce good results.

Previously, the realization of a friction drive motor with a surface acoustic wave at high frequency—e.g. 10 MHz—was considered to be almost impossible due to the small vibration amplitude around 10 nm. However, the difficulty of the friction drive has been overcome by control of the contact pressure between a slider and a stator. Kurosawa *et al* have proposed an X–Y linear motor that operates at 10 MHz in two dimensions and uses an $LiNbO_3$ wafer three inches in diameter [1]. We have already demonstrated the operation of an HF band (3 to 30 MHz) ultrasonic motor at 10 MHz [2] and 20 MHz [3, 4], which was made possible by operating the Rayleigh wave; a kind of surface acoustic wave was applied to the ultrasonic motors.

At high-frequency operation, vibration amplitude is very small. Hence, high contact pressure of, for example, several hundred MPa is required for the friction drive to avoid the influence of a squeeze film of air. The operation conditions and basic performance of ultrasonic motors under high-frequency operation have been investigated experimentally [5, 6]. The most significant result of this research was the discovery of the high output force density of the friction drive. The output force density was 50 N mm^{-2}. However, the actual output force was 1 mN because the tested slider was one steel ball. The maximum speed and maximum acceleration were 0.8 m s^{-1} and 900 m s^{-2}.

For a small linear actuator, the surface acoustic wave motor has numerous advantages, including high output force, high speed, long stroke up to centimeter order, high energy density, easy holding and high-resolution positioning. While the advantages of a linear motor have been well demonstrated, the motor itself remains to be developed.

As a first step in development of an actual linear motor, newly designed multi-contact-point sliders [7] were examined to determine whether they could provide sufficient thrust for practical use. A simplified simulation model [8] was used to estimate the available thrust. The result showed that a surface acoustic wave motor has significantly high potential to serve as small linear motor.

2. Experimental set-up

Figure 1 shows the schematic shape of a surface acoustic wave linear motor. A stator transducer is a rectangular piezoelectric plate. At both ends of the plate, interdigital transducers are arranged to excite the Rayleigh wave. One IDT is used to propagate the traveling wave. For this purpose, at the end of the plate, the wave is absorbed mechanically or by mechanical–electrical conversion. With the elliptical motion of the surface particles of the stator, a slider pushed to the stator is driven by the frictional force. The slider moves to the driving IDT.

The stator transducer material is 128 degree rotated Y-cut X-propagation $LiNbO_3$. The dimensions are shown in

† E-mail address: mkur@pe.u-tokyo.ac.jp

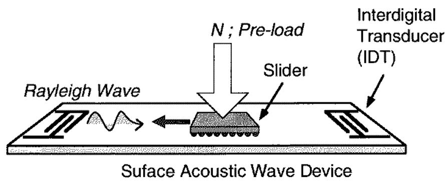

Figure 1. Schematic shape of a surface acoustic wave linear motor.

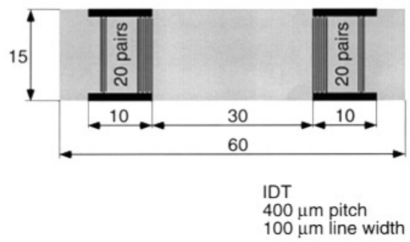

Figure 2. Surface acoustic wave device for the stator transducer.

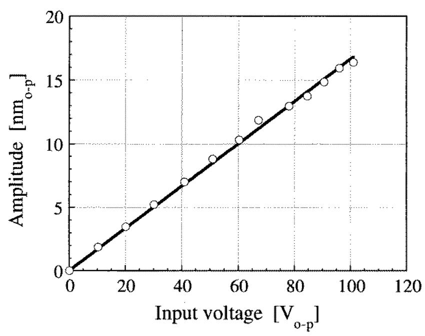

Figure 3. Vibration amplitude (normal direction) of the stator transducer shown in figure 2.

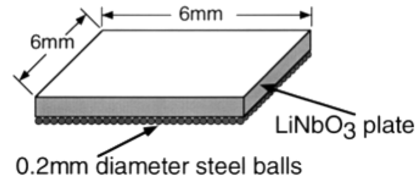

Figure 4. Scheme of the multi-contact-point slider using miniature steel balls.

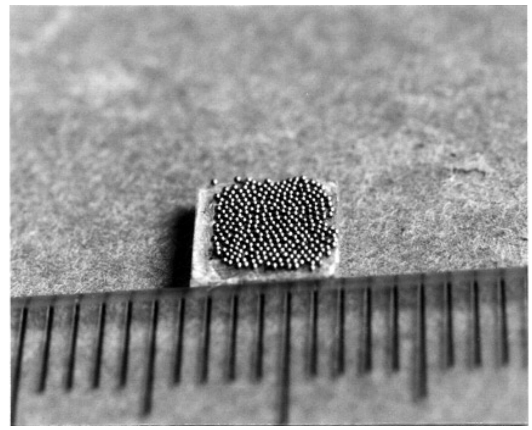

Figure 5. Photograph of the slider contact surface: steel ball diameter is 0.2 mm.

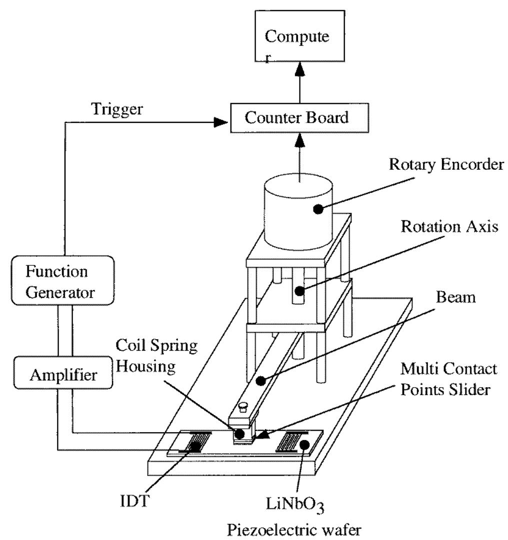

Figure 6. Scheme of the experimental set-up for the surface acoustic wave linear motor using a swing arm.

figure 2. The line width and pitch of the IDT were 100 μm and 400 μm. The resonance frequency was 9.6 MHz to propagate the Rayleigh wave. The conductance of the IDT was 20 mS at the resonance. The vibration displacement amplitude in normal direction to the surface was measured with a laser Doppler vibrometer as shown in figure 3. The tangential direction vibration velocity is also indicated in the graph.

In the case of a flat contact surface slider, the influence of the squeeze film pressure of the air is significant. Hence, a multi-point contact slider is necessary for good tribological conditions for the friction drive. Each fine contact point has so much high contact pressure that the squeeze film is broken. From the Hertz contact theorem, the contact area radius is a few μm and the contact pressure is several hundred MPa or more.

We used a mirror-finished 6×6 mm^2 flat surface $LiNbO_3$ plate and 500 0.2 mm diameter steel balls or 1200 0.1 mm diameter steel balls for the sliders. The steel balls were glued on the plate as illustrated in figure 4. The required uniformity of the contact points was of the order of nanometers, although the tolerance of the steel balls was of the μm order. Therefore, the differences of the steel ball diameters were adjusted by the thickness of the glue layer. Further, the elasticity of the glue was used for automatic adjustment of the uniformity of the contact points. The contact surface of a slider made up of 0.2 mm diameter steel balls is shown in figure 5.

The force of pressing slider against the stator, namely, the pre-load, was evaluated from the elastic deformation due to the normal force between the slider and the stator. Previous experiments have shown that the optimum depression is half of the vibration displacement [6]. For example, when the slider was a 1 mm steel ball and the vibration amplitude was 18 nm, the optimum pre-load

Table 1. Comparison of the multi-contact-point slider with steel balls.

Diameter of steel ball	[mm]	0.2	0.1
Number of steel balls		500	1200
Pre-load for each steel ball	[mN]	2.7	2.3
Elastic deformation (vibration amp. = 17 nm)	[nm]	9	9
Pre-load for slider	[N]	1.4	2.7
Maximum contact pressure	[MPa]	790	1200
Contact area of slider	[$mm^2 \times 10^{-3}$]	2.5	3.4
Maximum output force (expected values)	[N]	0.3	0.5
Output force per unit area (expected values)	[$N\ mm^{-2}$]	110	160

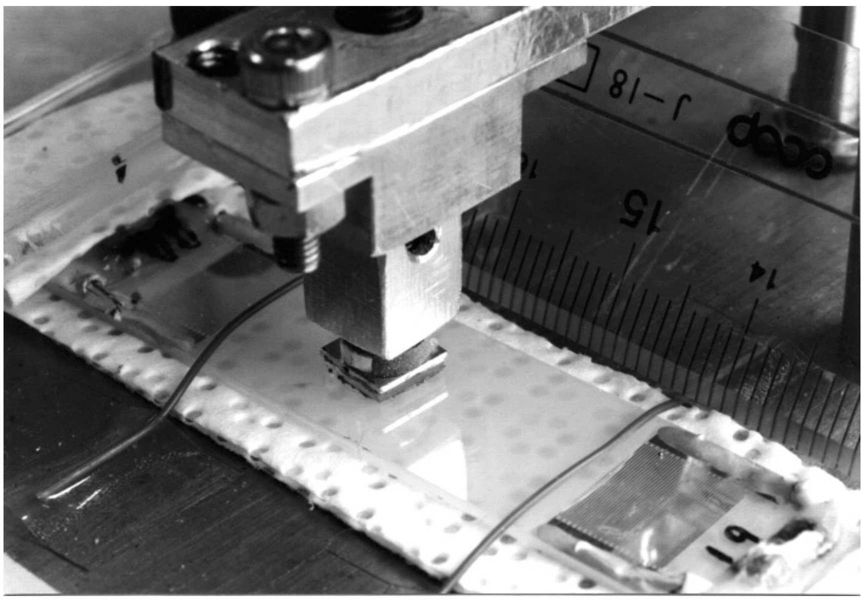

Figure 7. Close-up of the stator and the slider of the experimental set-up.

was 7 mN, which gave a suitable depression of 9 nm, as indicated in table 1 [2, 6]. In the case of a 0.2 mm steel ball slider, the optimum pre-load was calculated to be 2.7 mN for each steel ball, and 1.4 N for the slider. The whole contact area of the slider was 2.5×10^{-3} mm^2, or less than 1/10 000 of the plate area. The maximum contact pressure was 790 MPa at the center of each contact point. From the pre-load of 1.4 N and the friction coefficient of 0.2, the estimated driving force was about 0.3 N. Regarding the 0.1 mm steel ball, the optimum pre-load was calculated to be 2.3 mN for each steel ball, and 2700 mN for the slider. The whole contact area of the slider was 3.4×10^{-3} mm^2, namely about 1/10 000 of the plate area. The maximum contact pressure was 1200 MPa at the center of each contact point. From the pre-load of 2.7 N and using a friction coefficient of 0.2, the estimated driving force was about 0.5 N. These results are summarized in table 1.

Next, we carried out an experiment using the swing-arm type surface acoustic wave motor shown in figure 6. Using this apparatus, the linear motion of the multi-contact-point slider was changed to swing motion of a beam. Since the length of the swing arm was 5 cm and the traveling distance was about 2 cm, the curvature was not a problem.

The swing angle of the beam was measured with a rotary encoder. A coil spring set in a spring housing pressed against the multi-contact-point slider. The pre-load was changed from 0.3 N to 3.2 N. A photograph of the experimental set-up is shown in figure 7.

3. Experimental results

The driving frequency was 9.6 MHz and the voltage was 100 V_{o-p}. At this condition, the vibration amplitude was 17 nm. Figure 8 shows the transient response of the 0.2 mm steel ball slider to change of pre-load. These measured data were used to calculate the transient speed of the slider, as shown in figure 9. The acceleration of the slider at starting gives the maximum output force at each pre-load condition.

From these measurements, the output force was estimated as shown in figures 10 and 11. Figure 10 shows the output force as a function of the pre-load when the ball size was 0.2 mm diameter. The output force increased up to the optimum pre-load of 1.4 N. Since the optimum depression is half of the vibration displacement, the pre-load gave the depression of 9 nm. Then, beyond the optimum pre-load condition, the output force decreased. In this experiment, the maximum driving force was 0.3 N when the pre-load was about 1.4 N. These values were almost the same as the calculated values for each ball.

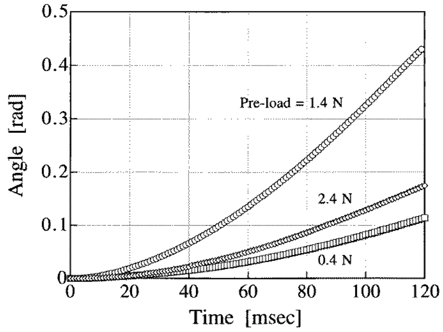

Figure 8. Experimental results of the multi-contact-point slider (0.2 mm diameter balls) transient response.

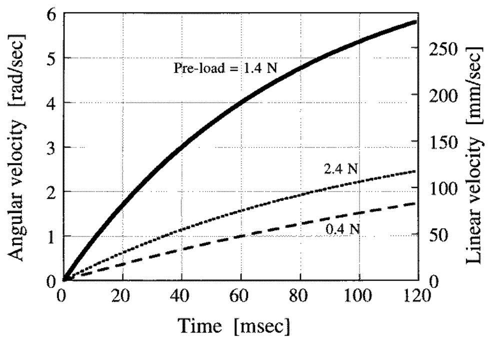

Figure 9. Transient responses of the slider speed estimated from the data in figure 8.

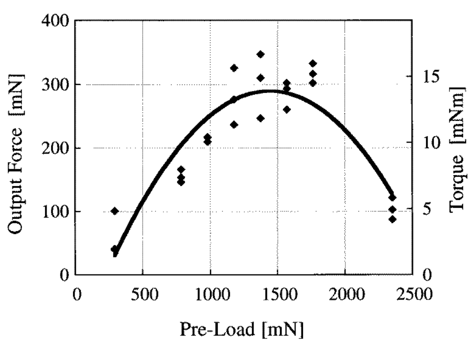

Figure 10. Thrust of the motor against the pre-load: contact ball diameter is 0.2 mm.

On the other hand, when the ball was 0.1 mm in diameter, the output force increased up to a maximum set-up pre-load of 3.2 N. The maximum driving force was 0.45 N when the pre-load was 3.2 N. These values were slightly different from the calculated values. The experimental results for the multi-contact slider are summarized in table 2.

The resolution of the stepping motion of the slider with a burst drive—i.e., the short duration drive time—we also measured. The driving voltage was maintained at 100 V_{o-p}. The play of the spring housing was larger than the micro-motion of the slider. Hence, the step motion distances of the slider, not the arm, are shown in figure 12. A laser heterodyne displacement measurement apparatus with a 4 nm resolution was used. The motor was found

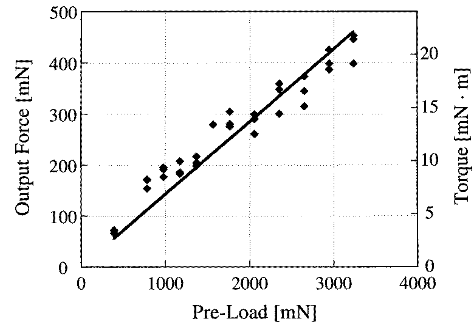

Figure 11. Thrust of the motor against the pre-load: contact ball diameter is 0.1 mm.

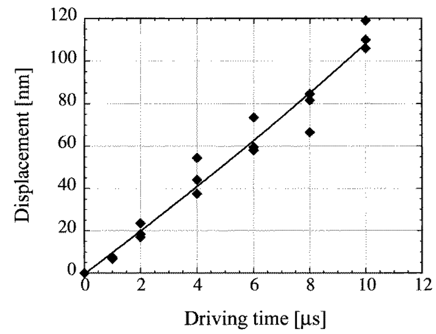

Figure 12. Movement of the motor against the stepping drive.

to have a very fine resolution with a precision of 10 nm or more.

The output force of 0.45 N is a large value in comparison with the stator and slider weights of 4 g and 0.2 g. If we ignore the extra weight of the experimental setup, the output force is 10 times the stator, 200 times the slider, weight-of-gravity. In these experiments, the contact areas constituted less than 0.01% of the surface area of the slider. By improving the geometrical design of the slider, a contact area of 0.1% can be achieved. In such a case, provided that the elastic vibration does not attenuate substantially due to the high mechanical impedance of the Rayleigh wave, we might obtain a much larger thrust of up to several newtons using an actuator of the same dimensions.

4. Simulation model

Assuming a simple one dimensional linear elasticity, the contact force will be in proportion to the deformation of the slider and the stator. Due to the high vibration frequency, the slider would be suspended at constant normal position. Images of the motion of the slider and stator are presented in figure 13. The interesting point is that the stator and the slider are deformed by a pre-load of the same order as the wave deformation.

The normal force, namely the pre-load, is estimated at the first step and used to obtain a traction force that is proportional to the pre-load. Here, the friction coefficient μ is assumed to be constant. To simplify the problem, it

Table 2. Experimental results of the multi-contact-point slider with small steel balls.

Diameter of the ball	[mm]	1	0.2	0.1
Number of steel ball(s)		1	500	1200
Speed	[mm s^{-1}]	440	350	300
Maximum output force	[mN]	0.95	300	450
Output force per unit area	[N mm^{-2}]	50	110	130

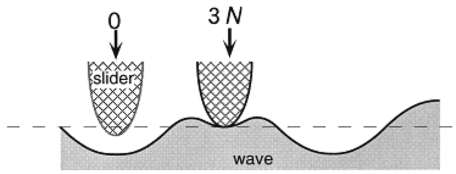

Figure 13. Scheme of the contact condition of the slider tip to the stator wave.

is assumed that the flowing power is much larger than the consumed power at the slider; that is, that the attenuation of the wave is negligibly small.

The normal vibration displacement is expressed as $u = a \sin \omega t$. For the sake of simplicity, the slider moves from left to right in figure 13. At a critical point of $\omega t = \phi$, the slider begins to contact the stator, and stops contacting at $\omega t = \pi - \phi$. Therefore, the pre-load varies temporally as $f_n = k(a(\sin \omega t - \sin \phi) + d)$, where f_n, k and d are the pre-load, the elastic constant at the contact part and the deformation at the bottom of the wave. The average of the f_n gives the static pre-load N.

The temporal driving force f_τ is proportional to the pre-load f_n; $f_\tau = \mu f_n$. The output force is obtained as follows:

$$F = \mu \int_{\phi}^{\varphi} -f_n \,\mathrm{d}t + \mu \int_{\varphi}^{\pi-\varphi} f_n \,\mathrm{d}t + \mu \int_{\pi-\varphi}^{\phi} -f_n \,\mathrm{d}t$$

where φ gives the slider speed v: $v = v_0 \sin \varphi$. If the slider speed is lower than $v_0 \sin \phi$, $\varphi = \phi$ in the above integral. Using these equations, the pre-load and the traction were calculated as indicated in figures 14 and 15. The phase angle corresponds to the temporal in actuality in these figures. Figure 14 shows the case wherein the slider contacts the stator during that half of the vibration cycle having no output force from the motor. Figure 15 indicates the case wherein the slider contacts the stator throughout the whole cycle.

The no-load speed and the maximum output force of the motor depend on the contact duration, as shown in figure 16. If the duration of contact is less than one-quarter of the whole vibration cycle, then a small thrust results in spite of the high speed. To maximize the output force, the slider should contact the slider throughout the whole vibration cycle, provided the contact area is the same, even though, in this case, the no-load speed is almost 70% of the vibration velocity. As mentioned above, when the vibration amplitude is 17 nm at 9.6 MHz, the vibration velocity of the normal direction and the tangential direction are 1 m s^{-1} and 0.7 m s^{-1} (figure 3). From the simulation, the no-load speed becomes 0.48 m s^{-1}. On the other hand, the

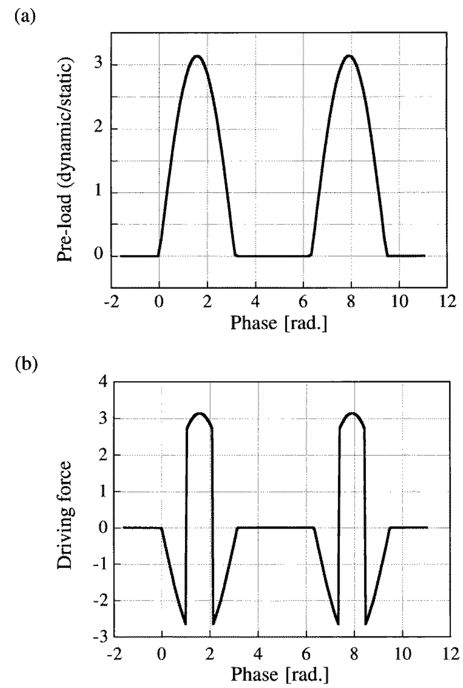

Figure 14. Pre-load wave form (a) and traction force (b) when the contact duration is a half cycle of the vibration.

experimental result under an apparently identical pre-load condition, i.e., the depression was half of the vibration amplitude, was 0.43 m s^{-1} [6]. The efficiency also merits further consideration. An example of a set of motor load characteristics is shown in figure 17.

5. Estimation and discussion

Our major interest in the simulation is to know the power consumption at the friction drive surface for evaluation of the output force. If the output power from the elastic wave through the friction is not a small value as against the transmitting power, the thrust of the slider might be limited to be a very small value. Otherwise, when the output force of the slider is a relatively large value, the vibration amplitude under the slider will remain almost constant irrespective of whether the wave is in front or back. Therefore, several cases of the pre-load were estimated, as shown in table 3.

Using the same transducer as above, the driving voltage was fixed at 100 V_{o-p} for the estimation. At this condition, the input power is 100 W because the conductance of the IDT is 20 mS. The wave propagates in both directions from

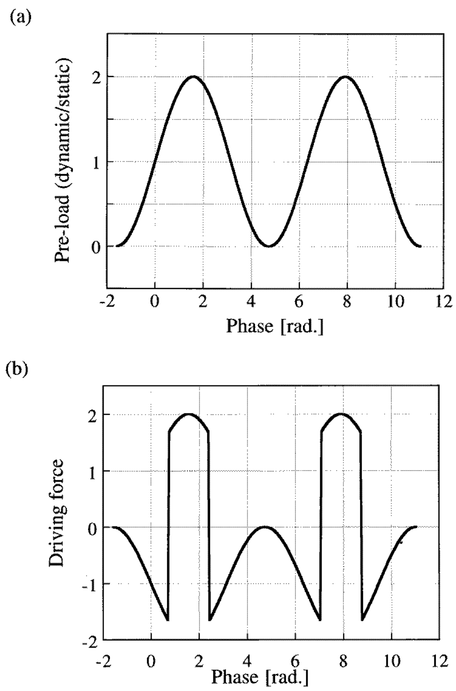

Figure 15. Pre-load wave form (a) and traction force (b) when the contact duration is a whole cycle of the vibration.

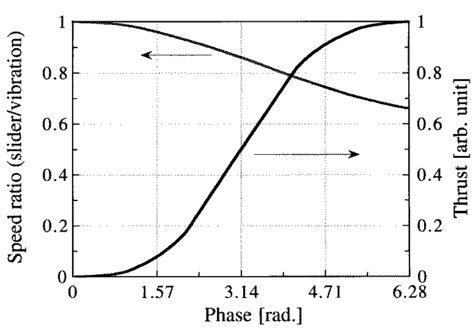

Figure 16. No-load speed and thrust of the motor against the contact duration of the vibration cycle.

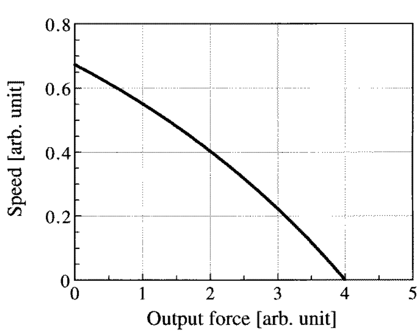

Figure 17. Simulated load characteristics of the surface acoustic wave linear motor.

the IDT, so that half of the 50 W power is available for the motor operation. Since the efficiency of the transduction from electrical power to mechanical vibration in IDT is very high, the loss in this part is negligible.

If the geometry of the contact point is the same, the thrust and the power consumed by friction are proportional to the contact area. In the case of the slider with 0.2 mm diameter steel balls used in section 3, the thrust and the consumed power were estimated to examine the availability of the output force. The results are summarized in table 3. The experimental output force was 0.3 N. At this condition, the consumed power was very small, so that we could not measure the change of the voltage of the IDT at the other end with or without the slider. Based on the calculation, the consumed power was only 0.2 W. This power is very slight in comparison with the flowing power of 50 W. Thus it was not possible to measure the attenuation of the wave.

If the contact area is ten times the slider surface used in the experiment by increase in contact point density, the pre-load and the thrust would increase ten times. Even in such a case, the consumed power will be only 2.2 W. To obtain the output force of 10 N, a pre-load of 46 N is required. At this condition, the consumed power is 7.3 W, as indicated in table 3. The attenuation of the wave at the slider is only about 8%. Based on the simulation results, then it is possible to obtain the significantly large output force of 10 N using the small stator transducer used herein.

The maximum speed of the motor is limited by the vibration velocity of the surface particles of the stator transducer. The limit of the vibration velocity of the $LiNbO_3$ was reported to be 3 m s^{-1} [9] or more. From this value, we obtained a tangential direction vibration velocity of more than 2 m s^{-1}. Hence, the experiment and the simulation results predict that the maximum speed would be 1.5 m s^{-1} or more.

One of the authors has already succeeded in circulation of the power flow in a vibration system of a traveling wave type linear motor having two longitudinal vibrators and a flexural vibrating bar for a wave guide [10] using an electrical circuit [11]. Hence, the circulation of the power will be available. The efficiency of the motor should be discussed after the achievement of the circulation of power. Otherwise, the efficiency is less than 1%.

Wear is always an important subject in the development of an ultrasonic motor. From the tribological point of view, this motor is advantageous in that the vibration amplitude is of the order of 10 nm. Hence, the slip between the stator and the slider is very small in one vibration cycle. In fact, we heard no noise at all from the motors in these experiments, possibly as a result of the small vibration amplitude drive. Since the contact pressure of this motor is large enough to deform the slider and the stator into the same order of the vibration amplitude, the deformation of the tangential direction, namely, the driving direction, would be able to reduce the slip. This difference of the tribological matter from that of other ultrasonic motors is an interesting subject from the viewpoint of the wear.

6. Conclusion

We have succeeded in enhancing the output force of the surface acoustic wave motor. To enlarge the contact area and the pre-load, a multi-contact-point slider was used. The thrust of each contact point of the slider was successfully concentrated. The maximum thrust was 0.3 N using 0.2 mm

Table 3. Thrust and consumed power of the enhanced contact area sliders.

	Pre-load [N]	Thrust [N]	P_{tr} [W]
Experiment ϕ0.2 × 500 (contact area: 0.01%)	1.4	0.3	—
Calculation			
same as exp.	1.4	0.3	0.22
area × 10	14	3	2.2
area × 33	46	10	7.3

diameter steel balls and 0.45 N using 0.1 mm diameter steel balls for contact points.

The simulation results predicted that a much larger thrust would be available by increasing the contact points without changing the slider and the stator dimensions. The calculated output force was 10 N, roughly twenty times that observed experimentally. To realize the required stator texture of the contact surface, silicon micro-machining techniques or other conventional methods would be applicable.

Acknowledgments

The authors thank Mr Y Ohtsuka of Dennso Co., Ltd, and Mr O Shinoura of TDK Co. for their cooperation in fabricating the surface acoustic wave transducers. The authors also appreciate Mr N Osakabe's help in measuring the data. This work was supported by a grant-in-aid for general scientific research from the Ministry of Education, Science, Sports and Culture of Japan.

References

[1] Kurosawa M, Takahashi M and Higuchi T 1994 Ultrasonic *X–Y* stage using 10 MHz surface acoustic waves *Proc. IEEE Int. Ultrasonics Symp. '94 (Cannes, 1994)* pp 534–8

[2] Kurosawa M, Takahashi M and Higuchi T 1996 Ultrasonic linear motor using surface acoustic waves *IEEE Trans. Ultrason. Ferroelectr. Frequency Control* **UFFC-5** 901–6

[3] Kurosawa M, Takahashi M and Higuchi T 1996 Operation condition and output force of surface acoustic wave motor *Technical Report* Institute of Electronics Information and Communication Engineers US96-76, pp 43–50 (in Japanese)

[4] Kurosawa M, Takahashi M and Higuchi T 1997 A surface acoustic wave motor using V-shape groove guide *Trans. Inst. Electron. Information Commun. Eng.* A **J80-A** 1711–7 (in Japanese)

[5] Takahashi M, Kurosawa M and Higuchi T 1995 Direct frictional driven surface acoustic wave motor *Proc. Int. Conf. on Solid-state Sensors and Actuators, Transducers 95 (Stockholm, 1995)* pp 401–4

[6] Kurosawa M, Takahashi M and Higuchi T 1996 Optimum pre-load of surface acoustic wave motor *Proc. IEEE International Ultrasonics Symp. '96 (San Antonio, TX, 1996)* pp 369–72

[7] Chiba M, Takahashi M, Kurosawa M and Higuchi T 1997 Evaluation of a surface acoustic wave motor output force *Proc. IEEE Workshop on MEMS (Nagoya, 1997)* pp 250–5

[8] Kurosawa M, Takahashi M and Higuchi T 1997 Contact and driving condition of a surface acoustic wave motor *Proc. IFAC Conf. on Control of Industrial Systems (Belfort, 1997)* pp 396–401

[9] Hirose S, Nakamura K, Adachi Y and Shimizu H 1991 Vibration level dependence of longitudinally vibration rectangular bar resonator using $LiNbO_3$ crystals *Proc. Annu. Meeting Acoust. Soc. Japan (1991)* pp 845–6 (in Japanese)

[10] Kurosawa M and Ueha S 1989 High speed ultrasonic linear motor with high transmission efficiency *Ultrasonics* **27** 39–44

[11] Kuribayashi M and Ueha S 1985 Study of ultrasonic linear motor IV–electrical method of energy back flow *Proc. Annu. Meeting of Acoust. Soc. Japan (1985)* pp 585–6 (in Japanese)